Supporting Information

The Bright Future for Electrode Materials of Energy Devices — Highly Conductive Porous Na-Embedded Carbon

*Wei Wei[†], Liang Chang[†], Kai Sun[‡], Alexander J. Pak[§], Eunsu Paek[§], Gyeong S. Hwang[§], and Yun Hang Hu[†,]**

[†]Department of Materials Science and Engineering, Michigan Technological University, 1400 Townsend Drive, Houghton, MI 49931-1295, USA

[‡]Department of Materials Science and Engineering, University of Michigan, Ann Arbor, MI 48109-2136, USA

[§]Department of Chemical Engineering, University of Texas at Austin, Austin, TX 78712-1589, USA

*Author to whom correspondence should be addressed. E-mail: yunhangh@mtu.edu

1. Experimental Section

Synthesis and characterization of Na-embedded carbon materials: 50 mmol sodium (Na) powder (Aldrich) was loaded into a ceramic tube batch reactor and CO was introduced into the reactor with initial pressure of 50 psi at room temperature, followed by heating the reactor to a selected temperature (550, 600, or 650 ^{o}C) at a rate of 10 ^{o}C min^{-1} and then keeping the reaction for 48 hours. The obtained Na-embedded carbon material (Na@C) was separated from other products by 36.5 wt% hydrochloric acid (HCl) treatment, de-ionized (DI) water washing (more than 10 times), and centrifugation separation. The Na@C was dried overnight at 80 ^{o}C. The obtained Na@C materials were subjected to X-ray diffraction (XRD) measurements using a Scintag XDS-2000 powder diffract meter with Cu Kα (λ=1.5406Å) radiation. Their structures were characterized by Hitachi-4700 field emission scanning electron microscope (FESEM) with energy dispersive spectroscopy (EDS), JEOL JEM-3100R05 transmission electron microscope (TEM), and Raman spectrometer (Olympus BX41) with a helium-neon laser to excite the samples. Their compositions were determined by the elemental analysis (the Control Equipment Corporation Model 240XA) and the inductively coupled plasma (ICP) optical emission spectrometry (OES) (PerkinElmer Optima 7000 DV ICP-OES). X-ray photoelectron spectra (XPS) were collected (for structure and composition analysis) using a Kratos Ultra AXIS DLD XPS with a monochromated Al source. Their surface areas and pore size distributions were measured by nitrogen adsorption at liquid-nitrogen temperature (77K) using a Micromeritics ASAP 2000 Adsorption Instrument. Their conductivities were determined by Jandel four-point system (RM3 test unit).

Accessible surface area measurement: The electrodes were fabricated by mixing Na@C samples, carbon black, and poly(tetrafluoroethylene) with a weight ratio of 80:10:10 in isopropyl alcohol to form a homogeneous slurry. Then, the slurry was rolled to a strip and pressed onto 1×1 cm^2

nickel foam, followed by drying at 100 ^{o}C for 24h. The symmetrical two electrode configuration, in which both the cathode and anode are Na@C electrodes (mass loading of about 4 mg/cm^{2}) with a separator (glassy microfiber filter GF/F) between them and electrolyte of 2 M KOH aqueous solution, was used for charge adsorption capacity tests. Galvanostatic charge/discharge cyclings were carried out with Princeton Potentiostat/Galvvanostat Model 273A electrochemical workstation at current density of 1 A g^{-1} for 0~1 V. The accessible surface areas for electrolyte ions were calculated from the charge adsorption capacities.

Fabrication and characterization of DSSCs: **(1)** ***Counter electrodes:*** The Na@C powder was mixed with alcohol with stirring for 5 min to form a homogeneous paste. Then, the paste was deposited on a clean FTO glass plate to form a film by the doctor-blade method, followed by drying at 80 ^{o}C for 4 hours. The thickness of the film, which was measured by Model 6000 micromanipulator testing station, is about 20 μm. Cyclic voltammetry measurements were used to evaluate the catalytic activity of the Na@C electrode using an electrochemical workstation (EG&G Princeton Applied Research) with a three-electrode system (Na@C as a working electrode, Pt wire as a counter electrode, and Ag/AgCl as a reference electrode) containing acetonitrile solution of 10 mM LiI, 1 mM I_2, and 0.1 M $LiClO_4$. **(2)** ***Photo electrodes:*** The conducting surface of the FTO was treated with a 40 mM $TiCl_4$ aqueous solution at 70 ^{o}C for 30 min, followed by forming a TiO_2 film with a commercial TiO_2 sol (Solaronix, Ti-Nanoxide T/SP) using the doctor-blade method. The TiO_2 film was thermally treated in air at 325 ^{o}C for 5min, 375 ^{o}C for 5 min, 450 ^{o}C for 15 min, and 500 ^{o}C for 15 min. The obtained TiO_2/FTO glass plate was post-treated with the 40 mM $TiCl_4$ solvent at 70 ^{o}C, followed by heating in air at 500 ^{o}C for 30min. Finally, the obtained film was immersed in a cis-bis(isothiocyanato) bis(2,2'-bipyridyl-4,4'-dicarboxylato)-ruthenium(II)-bis-tetrabutylammonium (N719, 0.3 mM in ethanol)

dye solution for 24 hours to achieve dye sensitization. **(3)** ***Fabrication and performance evaluation of DSSCs:*** The sandwich solar cells were assembled using the dye-sensitized TiO_2 photoelectrode and the Na@C counter electrode with liquid electrolyte (I^-/I_3^- redox) between them. The electrolyte consists of 0.025 M LiI, 0.04 M I_2, 0.28 M tert-butyl pyridine (TBP), 0.6 M 1-butyl-3-methylimidazolium iodide (BMII), and 0.05 M guanidinium thiocyanate in acetonitrile/valeronitrile solvent with 85/15 volume ratio. The effective cell area is 0.25 cm^2. The photovoltaic performance of the fabricated cells with photo masks was evaluated by Kithley 2400 under illumination of 100 mW cm^{-2} at the range of 320 nm - 1100 nm using a solar simulator (Newport). Electrochemical impedance spectroscopy (EIS) data of DSSCs were obtained at open circuit voltage and 10 mV amplitude over the frequency range of 0.1-100 kHz using CHI 660D electrochemical workstation under dark condition.

Fabrication and characterization of supercapacitors: Symmetrical two-electrode configuration was utilized to compare electrochemical performance of AC, CSG, and Na@C-550 electrodes, which consists two electrodes with mass loading of about 4 mg cm^{-2} as anode and cathode, a separator (Glassy microfiber filter GF/F) and electrolyte (2M KOH aqueous solution). Electrodes was fabricated as follows, activated materials, carbon black, and poly(tetrafluoroethylene) was mixed in isopropyl alcohol to obtain homogeneous slurry with mass ratio of 80:10:10. The slurry was rolled to a strip and press into nickel foam (1 cm^2). After fully drying at 100 ^oC oven overnight, Cyclic voltammetry (CV) test and galvanostatic charge/discharge cycling were carried out with Princeton Potentiostat/Galvanostat Model 273A electrochemical workstation.

Calculation method: **(1)** ***Na-embedded porous carbon structure generation:*** First, the amorphous graphitic carbon matrix was created using quenched molecular dynamics with interatomic interactions described by a Mimetic force field[1] using the LAMMPS[2] package. The

initial simulation domain consisted of a 2.5×2.5×2.5 nm^3 box with 750 C atoms arranged in a cubic lattice. Starting from a temperature of 18000 K, the simulation was quenched to 1000 K over 5.6 ns using a time step of 0.07 fs; the temperature was controlled using a Nosé-Hoover thermostat[3] with a damping factor of 1 ps. After quenching, dangling C atoms were removed until only sp^2 and edge carbon remained. The carbon structure was further relaxed using an isobaric-isothermal Nosé-Hoover barostat (thermostat) at 1 atm (300 K) with a damping factor of 10 ps (1 ps) and AIREBO force-field.[4] After relaxation, the final lengths of the box were 2.5097 nm with 710 C atoms. Finally, 8 Na atoms were placed along the surface; half of the atoms are situated in regions encapsulated by C while the other half are on the surface. **(2)** ***Electronic structure calculations:*** Geometry optimization and electronic structure calculations were performed using density functional theory within the Perdew-Berke-Ernzerhof generalized gradient approximation (GGA-PBE)[5] using dispersion corrections from the Grimme method (DFT-D2)[6] as implemented in VASP.[7] We employed the projector augmented wave (PAW) method[8] to describe the interaction between core and valence electrons, and a planewave basis set with a kinetic energy cutoff of 400 eV. Periodic boundary conditions were employed in all three directions. For the Brillouin zone integration, only the Γ point was used; all energy (force) calculations were converged to within 1×10^{-6} eV (0.02 eV/Å). **(3)** ***Adsorption calculations:*** For I_3^- adsorption energy calculations using VASP, a 5×3 rectangular supercell of graphene was used with the GGA-optimized lattice constant of 2.466 Å and periodic boundary conditions in all three directions; a vacuum spacing of 45 Å was used to avoid interactions with the periodic image. One Na and I_3^- molecule was placed on either side of the graphene sheet. Geometry optimization and energy calculations used a 2×2×1 Monkhorst-Pack mesh[9] All other details are described in the above section.

2. Thermodynamic evaluation

Gibbs free energy change and enthalpy change were calculated for the following reaction:

$$Na_{(l)} + 3/2\ CO_{(g)} \rightarrow C + 1/2\ Na_2CO_{3(s)}$$

As shown in Figure S1, one can see negative changes of Gibbs free energy and enthalpy, which confirm the thermodynamic spontaneity and energy-efficiency, respectively.

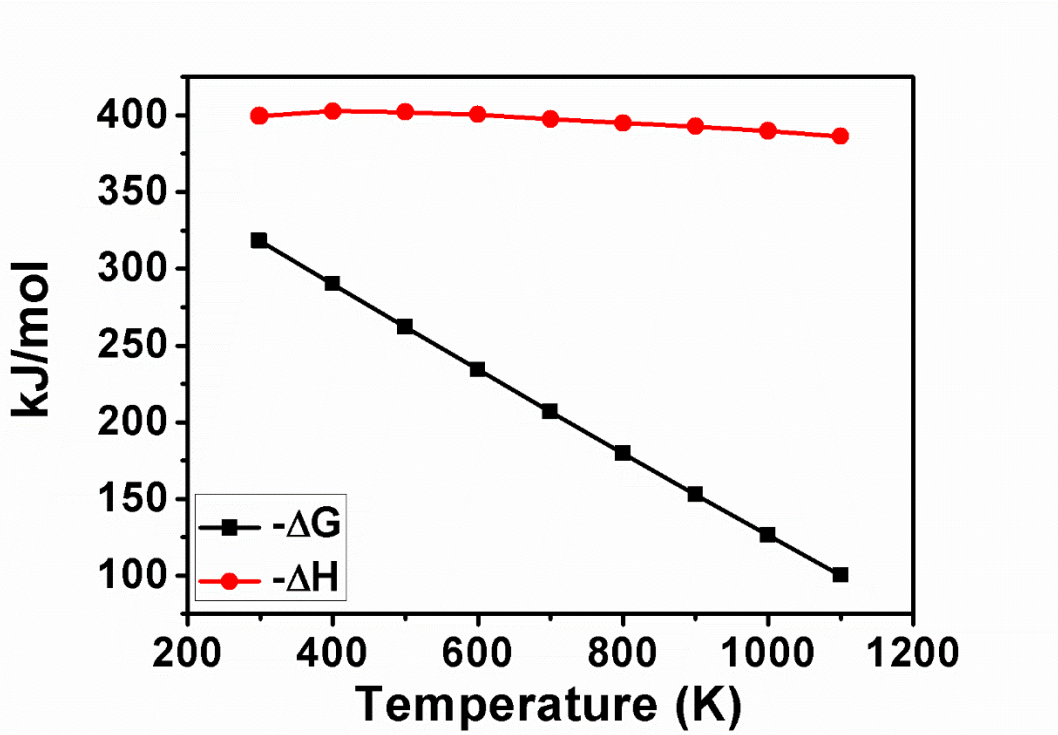

Figure S1. Thermodynamic calculations. Gibbs free energy change (ΔG) and reaction enthalpy change (ΔH) vs temperature for reaction between Na and CO to carbon and Na_2CO_3.

3. Characterization of solid products

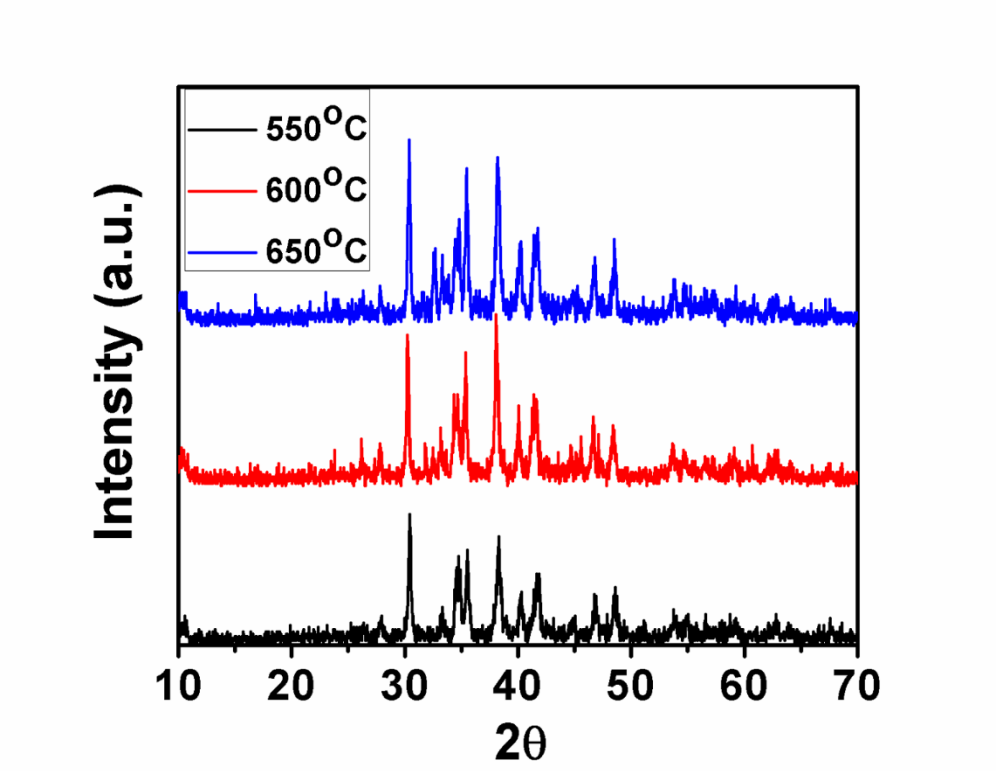

Figure S2. XRD characterization of solid products from the reaction between Na and CO at 550 °C, 600 °C, or 650 °C for 48 h. (The solid products were not subjected to any post-treatment).

4. Compositions of Na@C materials

Table S1. Composition (from Elemental Analysis and ICP) and electrochemical characteristics of Na@C samples.

Samples	Elemental Analysis		ICP	EIS		
	C (mol%)	O (mol%)	Na (wt%)	R_s (Ω)	R_{ct} (Ω)	Z_N (Ω)
Na@C-550	92.01	7.99	2.1	16	15	240
Na@C-600	92.89	7.11	2.7	16	14	220
Na@C-650	93 .05	6.95	1.8	17	15	250
Pt	-	-	-	21	25	280

Table S2. Carbon samples components from XPS measurements.

Samples	Sp^2 284.8eV	Sp^3 285.5eV	-C-O 286.7eV	-C=O 287.8eV	-O-C=O 288.9eV
Na@C-550	0.70	0.14	0.07	0.05	0.04
Na@C-600	0.73	0.15	0.08	0.03	0.01
Na@C-650	0.80	0.15	0.03	0.01	0.01

5. Pore size distributions

The pore size distributions of Na@C materials and activated carbon were calculated with BJH method from nitrogen adsorption at liquid nitrogen temperature. Shown in Figure S3, one can see that the pores in Na@C materials are mesopores and macropores, whereas the most of pores in activated carbon are micropores.

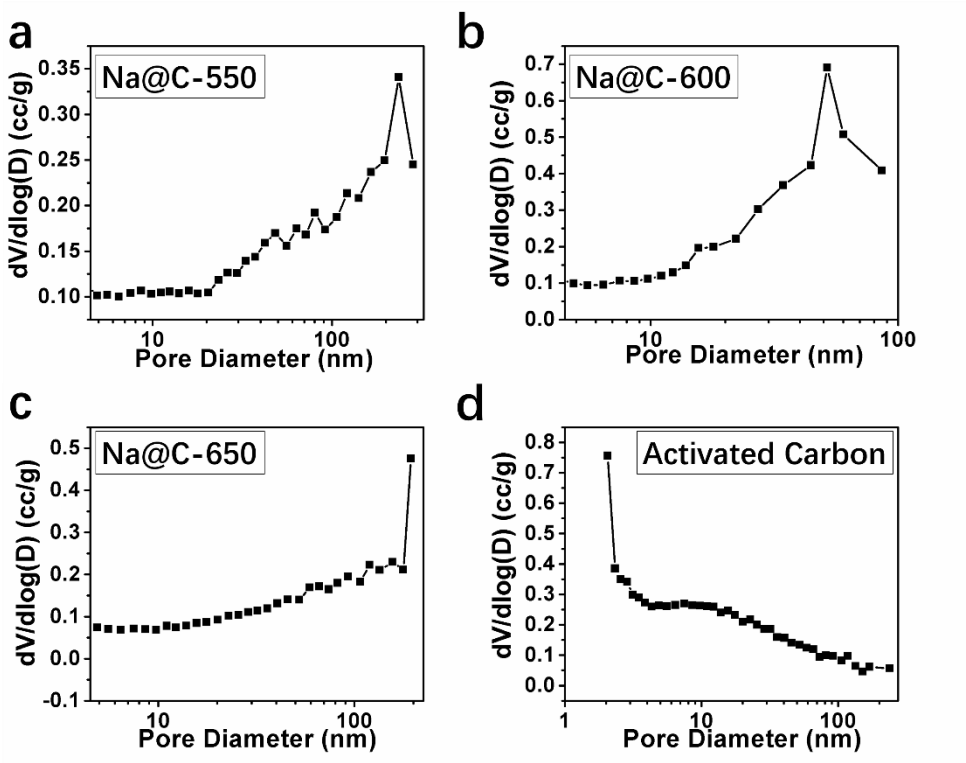

Figure S3. Pore size distribution of Na@C samples and activated carbon.

6. Total surface areas and accessible surface areas of Na@C materials

The total BET surface areas of Na@C material were obtained with BET model from measured by N_2 adsorption at 77K.

The accessible surface areas of Na@C materials to electrolyte ions were calculated as follows: Galvanostatic charge/discharge profiles were used to obtain specific capacitances (Figure S4). Furthermore, because the intrinsic capacitance of a perfect graphene sheet with surface areas of 2630 $m^2\ g^{-1}$ is 21 Uf cm^{-2},[10] a graphene sheet possesses specific capacitance of 526 F g^{-1} when its surface area is fully accessible to electrolyte. Therefore, we can calculate the accessible surface area of a carbon material to electrolyte from its specific capacitance with following equation:

$$\boldsymbol{accessible\ surface\ area} = \frac{\mathbf{2630}\left[\frac{m^2}{g}\right]\times\mathbf{120}\left[\frac{F}{g}\right]}{\mathbf{526}\left[\frac{F}{g}\right]} = \mathbf{600}\left[\frac{m^2}{g}\right] \qquad (1)$$

The obtained accessible surface areas are 600, 329, and 262 $m^2\ g^{-1}$ for Na@C materials synthesized at 550, 600, and 650 ^oC, respectively.

Table S3. BET surface area measured using nitrogen adsorption at liquid-nitrogen temperature (77K) and accessible surface area of Na@C sampels.

Samples	BET surface area ($m^2\ g^{-1}$)	Accessible surface area ($m^2\ g^{-1}$)
Na@C-550	625	600
Na@C-600	345	329
Na@C-650	301	262

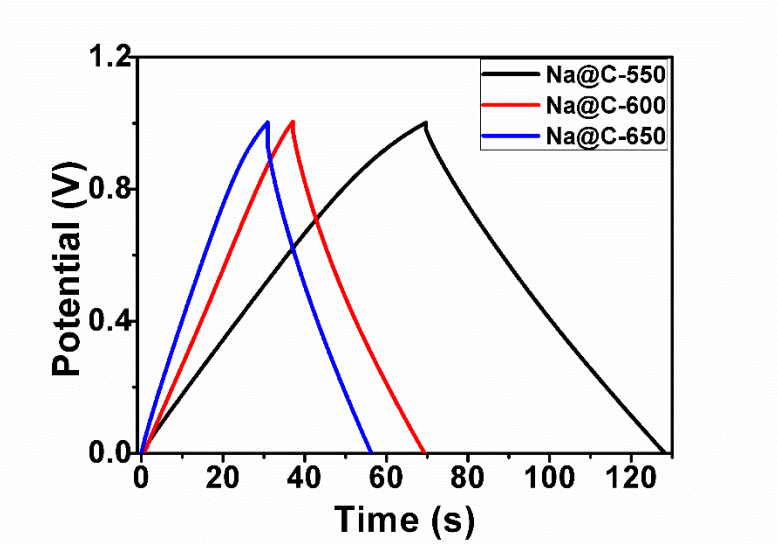

Figure S4. Galvanostatic charge/discharge profile of Na@C samples in 2 M KOH aqueous solution with symmetrical double layer capacitors.

7. Accessible surface areas of Pt film

The accessible surface area of a Pt film was determined by cyclic voltammograms (CV). The Pt film deposited on a FTO glass is electrochemically active in 0.5M H_2SO_4. Figure S5 shows hydrogen adsorption characteristics. The electrochemically accessible surface area was estimated by integrating the voltammogram corresponding to hydrogen desorption from the Pt surface. The obtained surface area is 0.0022 $m^2 g^{-1}$ Pt.

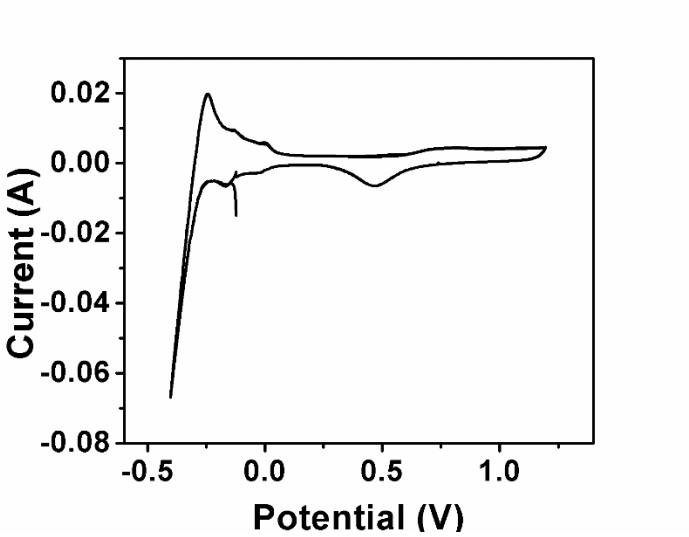

Figure S5. CV curve of Pt film in the solution of nitrogen saturated 0.5M H_2SO_4.

8. Theoretical prediction of band structures of C and Na@C materials

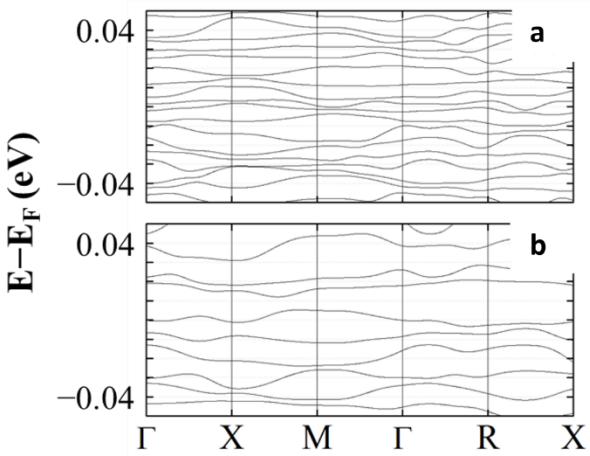

Figure S6. Theoretical prediction of band structures. (a) Band structure of bare porous carbon structure. (b) Band structure of porous carbon structure with 2 wt.% Na.

9. DFT calculation for I_3^- adsorption on Na@C

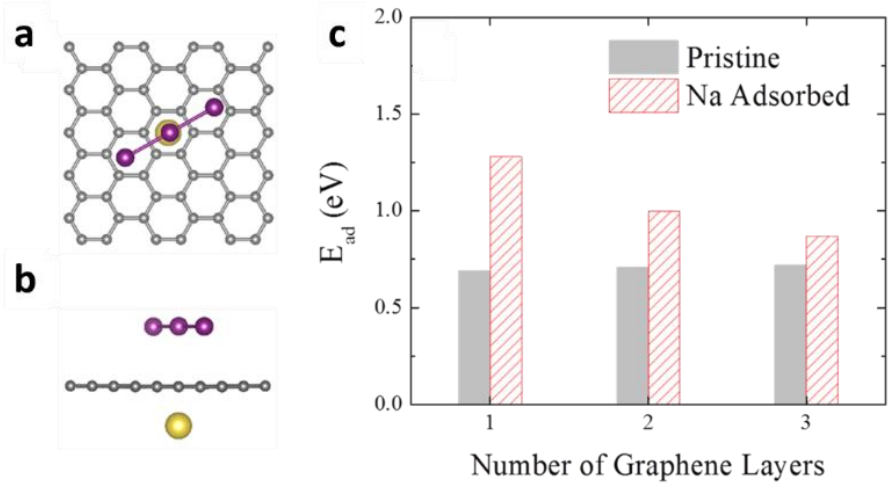

Figure S7. Adsorption of I_3^- on C and Na@C materials. (a) Top view of a schematic depicting the simulated adsorption of I_3^- (purple balls and sticks) on graphene (gray balls and sticks) with Na on the other side (yellow ball). (b) Side view of the same schematic. (c) Adsorption energy (E_{ad}) of I_3^- on graphene with the listed number of layers and in the absence and presence of Na.

10. IPCE spectra of DSSCs

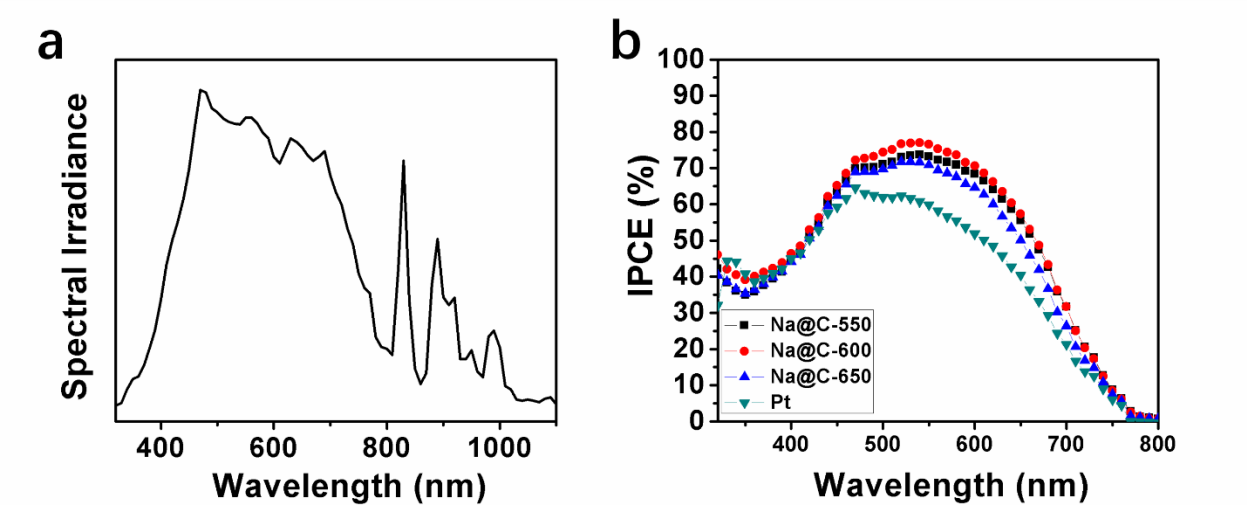

Figure S8. **(**a) Simulated 1.5G Sunlight Spectrum. (b) IPCE Spectrum. IPCE spectra of DSSCs with Pt, Na@C-550, Na@C-600, or Na@C-650 CEs.

Figure S8b shows the incident photon-to-current conversion efficiency (IPCE) spectra. Furthermore, it was found that the J_{sc} obtained from the I-V measurement is 0.4% higher in average than that calculated from the IPCE curves, which is in a reasonable range.[11] The discrepancy is due to the difference in illumination conditions. A single wavelength was used for measuring photoresponse in the IPCE test, whereas the I-V measurement was carried out under steady illumination of broadband light with a full spectrum.

11. Histogram of efficiencies

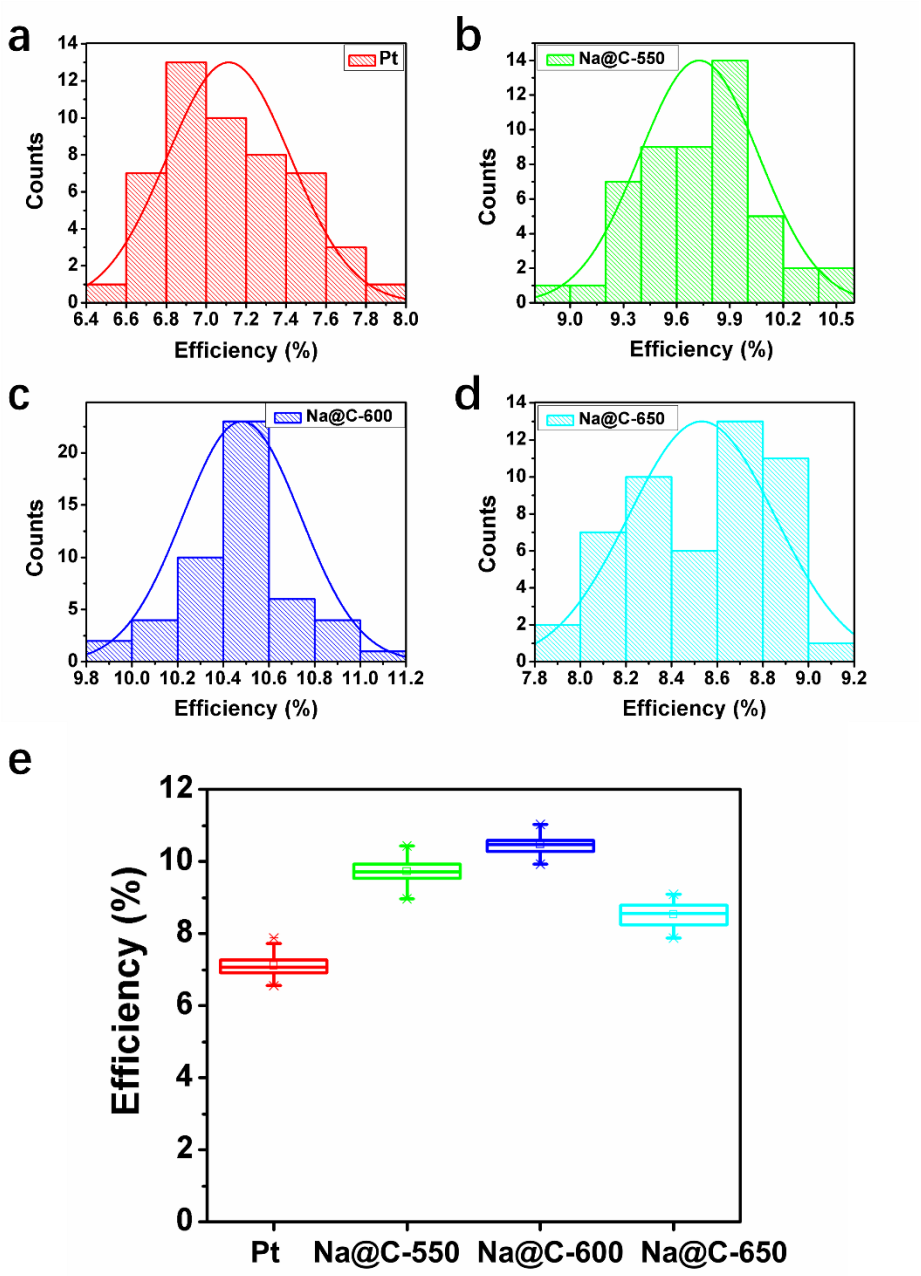

Figure S9. Histograms of efficiencies of power conversion (PCE) of 50 seperate DSSCs fabricated under the same experimental conditions with (a) Pt. (b) Na@C-550. (c) Na@C-600. and (d)Na@C-650 as counter electrodes. Efficiencies with error bars for those 4 types of DSSCs were summarized in (e).

12. Comparison between DSSCs with Na@C and 3D graphene as counter electrodes

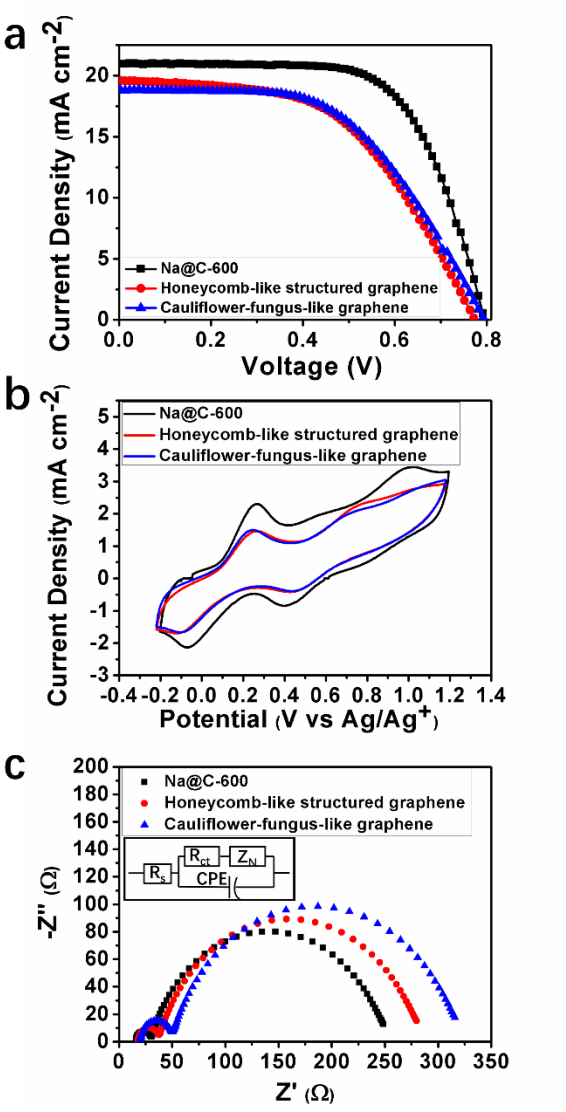

Figure S10. Characterization of DSSCs with various CEs. (a) Photocurrent density-voltage curves and performance parameters of DSSCs with Na@C-600, Honeycomb-structured graphene (HSG), and cauliflower-structured graphene (CSG) CEs under simulated 1.5G sunlight illumination. (b) CV curves of I_3^-/I^- redox pairs at Na@C-600, HSG, and CSG CEs at a scan rate of 20 mV s^{-1}. (c) EIS curves for cells fabricated with Na@C-600, HSG, and CSG CEs (the inset presents the equivalent circuit).

Table S4. Photovoltaic performance and electrochemical characteristics of DSSCs.

Samples	V_{oc} (V)	I_{sc} (mA cm^{-2})	ff	Efficiency (%)	R_s (Ω)	R_{ct} (Ω)	Z_N (Ω)
Na@C-600	0.80	20.95	0.66	11.03	16	14	220
Honeycomb-like structured graphene	0.77	19.60	0.52	7.90	18	19	245
Cauliflower-fungus-like graphene	0.79	18.82	0.54	8.07	20	29	270

13. Electrocatalytic evaluation and electrochemical impedance characterization

The catalytic activity of Na@C materials were further evaluated by cyclic voltammograms (CV) using a three-electrode electrochemical system, in which the Na@C materials were used as working electrodes, Pt wire as the counter electrode, Ag/Ag^+ as the reference electrode, and the solution of 10 mM LiI, 1 mM I_2, and 0.1 M $LiClO_4$ as electrolyte. Figure S11a shows all of the samples exhibited two pairs of redox peaks. The more positive pair corresponds to the redox reaction of I_2/I_3^-, while the more negative pair corresponds to the redox reaction of I_3^-/I^-. The electrochemical rate constant of a redox reaction is inversely proportional to the peak to peak separation (E_{pp}), which is the separation between the cathodic and anodic peak.[12] Among four electrodes (three for Na@C materials and one for Pt), Na@C-600 exhibited the smallest E_{pp} and the highest I_3^-/I^- redox current density (Figure S11a), confirming its largest intrinsic catalytic activity. In contrast, one can see the largest E_{pp} and the lowest I_3^-/I^- redox current density for the Pt electrode, indicating its smallest catalytic activity. Furthermore, the excellent stability of Na@C-600 electrode was demonstrated by the CV test of 500 cycles (Figure S12). In addition, CV curves also revealed higher electrocatalytic activity of Na@C-600

than that of 3D Na-free graphene (Figure S10b). Furthermore, DSSCs with Na@C counter electrodes were subjected to electrochemical impedance spectrum (EIS) characterization. As shown in Figure S11b, one can see two well-defined semicircles, which were quantitatively analyzed with an equivalent circuit (inset of Figure S11b), providing series resistance (R_s), charge-transfer resistance (R_{ct}) at the CE /electrolyte interface, and charge-transfer resistance (Z_N) at the TiO_2/dye/electrolyte interface (Table S1). The Na@C-600 electrode shows the smallest charge-transfer resistances (R_{ct} and Z_N), which depend on the catalytic reduction of I_3^- to I^-. This indicates that the Na@C-600 electrode possesses the highest catalytic activity. In contrast, the largest charge-transfer resistances (R_{ct} and Z_N) of Pt electrode can be attributed to its lowest catalytic activity. Those are consistent with CV measurements, which further confirm that Na plays an important role in Na@C CEs.

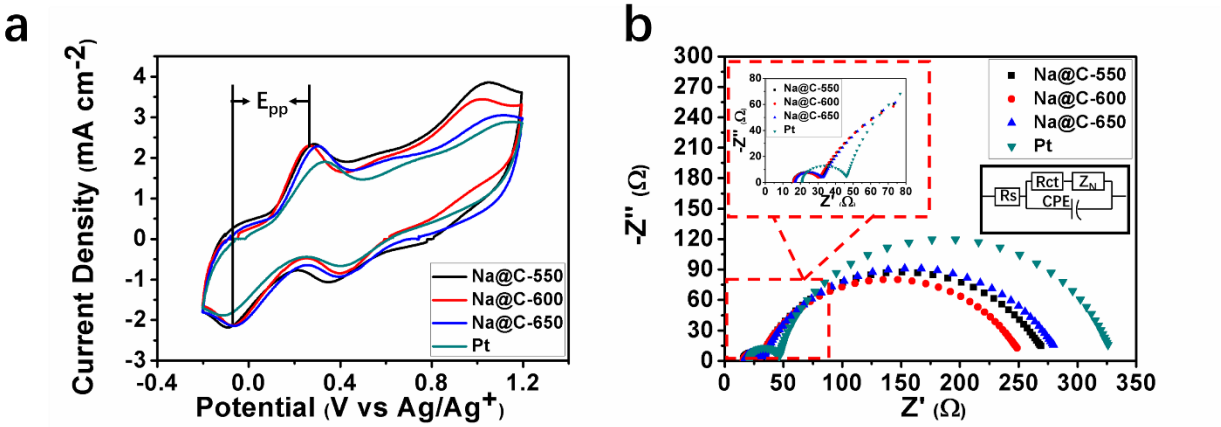

Figure S11. Characterization of DSSCs with Na@C CE. (a) CV curves of I_3^-/I^- redox pairs at Pt, Na@C-550, Na@C-600, and Na@C-650 CEs at a scan rate of 20 mV s^{-1}. (b) EIS curves for cells fabricated with Pt, Na@C-550, Na@C-600, and Na@C-650 CEs (the equivalent circuit is included as a inset).

14. Stability of Na@C counter electrode

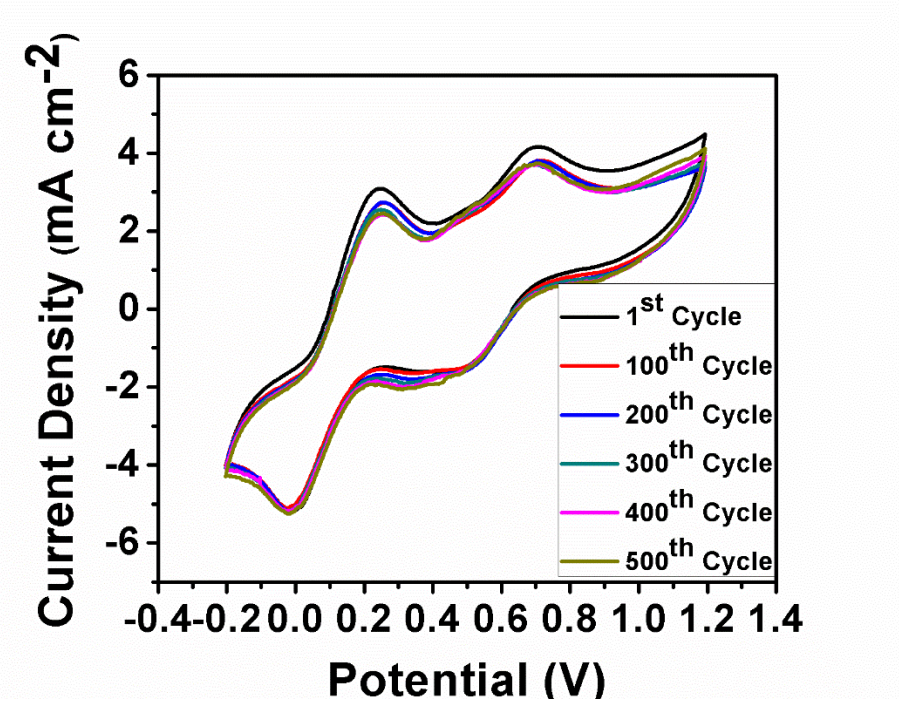

Figure S12. Stability evaluation of Na@C-600 in iodine electrolyte.

15. Explanation of counter-electrode-induced V_{oc}

The difference of open circuit voltages (V_{oc}) between DSSCs with Na@C and Pt counter electrodes (Figure 4a) can also be explain by charge-transfer resistance (Z_N) at the TiO_2/dye/electrolyte interface, which is proportional to changer recombination at the interface. The two possible factors can cause a change in V_{oc}: (1) a shift of the TiO_2 conduction band with respect to the electrolyte potential and (2) differences in the e^--TiO_2/electrolyte$^+$ recombination reaction.[13] The former one can be discarded, because the same photoelectrode and electrolyte were used for all DSSCs. Therefore, the V_{oc} increase of about 0.05 V, which was caused by replacing Pt CE with a Na@C electrode for a DSSC (Figure 4a), must be due to a decrease in the e^--TiO_2/electrolyte$^+$ recombination reaction. This is confirmed by EIS measurements, in which the DSSC with a Na@C CE exhibited a smaller charge-transfer resistance (Z_N) at the

TiO_2/dye/electrolyte interface than that with Pt CE. Furthermore, the effect of a counter electrode on the e^--TiO_2/electrolyte$^+$ recombination reaction can be explained as follows: The oxidized electrolyte (electrolyte$^+$) can be regenerated via two competitive reactions, namely, the e^--TiO_2/electrolyte$^+$ recombination reaction at the photoelectrode and the electrocatalytic reduction of electrolyte$^+$ at the counter electrode. A counter electrode with higher electrocatalytic activity should have a faster catalytic reduction of electrolyte$^+$, leading to a less chance for the e^--TiO_2/electrolyte$^+$ recombination reaction at the photoelectrode.

16. Application of Na@C and 3D graphene for supercapacitors

Three symmetrical double-layer capacitors were fabricated with Na@C-550, 3D cauliflower-structured graphene (CSG), and commercial activated carbon (AC), respectively. The electrochemical tests of those capacitors were conducted in 2 M KOH at potential range of 0~1 V. The results are shown in Figure S13.

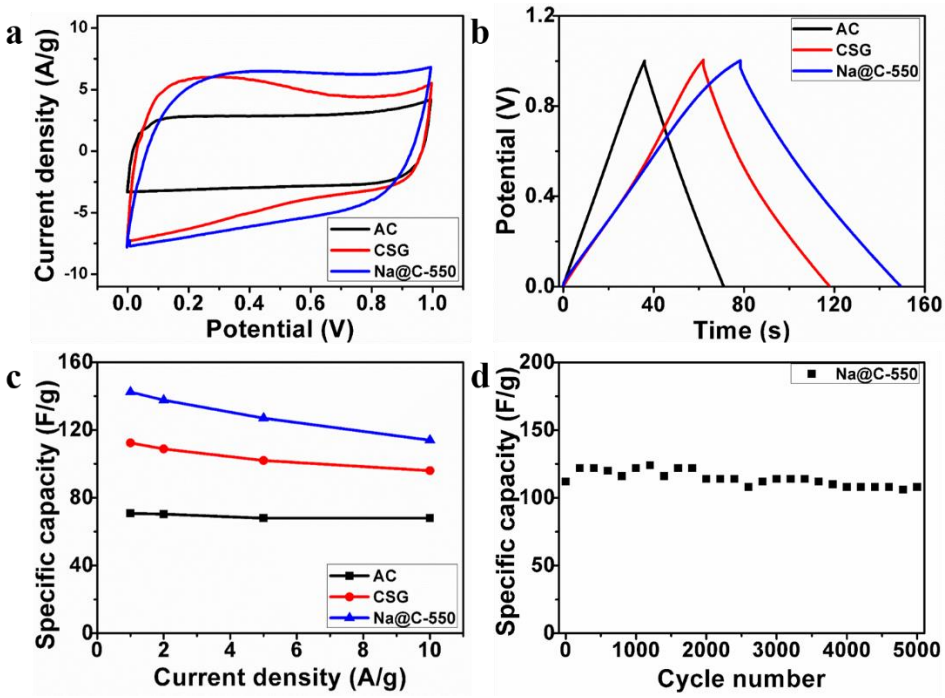

Figure S13. Electric double layer capacitor performance of Na@C-550, activated carbon (AC), and 3D cauliflower-structured graphene (CSG) in 2M KOH aqueous solution. (a) CV curves at scan rate of 100 mV s^{-1}. (b) galvanostatic charge/discharge profile at current density of 1 A g^{-1}, (c) specific capacity vs. current density, and (d) cycling performance of Na@C-500 at current density of 10 A g^{-1}. (Mass loading is 4.28mg cm^{-2} for Na@C electrode)

Supplementary Reference

(1) Shi, Y. *J. Chem. Phys*. **2008**, *128*, 234707-234717.

(2) Plimpton, S. *J. Comput. Phys*. **1995**, *117*, 1-19.

(3) Hoover, W. *Phys. Rev. A* **1985**, *31*, 1695-1697.

(4) Stuart, S. J.; Tutein, A. B.; Harrison, J. A. *J. Chem. Phys.* **2000**, *112*, 6472-6486.

(5) Perdew, J. P.; Burke, K.; Ernzerhof, M. *Phys. Rev. Lett.* **1996**, *77*, 3865-3868.

(6) Grimme, S. *J. Comput. Chem*. **2006**, *27*, 1787-1799.

(7) Kresse, G.; Furthmüller, J. *Phys. Rev. B. Condens. Matter*. **1996**, *54*, 11169-11186.

(8) Blöchl, P. *Phys. Rev. B* **1994**, *50*, 17953-17979.

(9) Monkhorst, H. J.; Pack, J. D. *Phys. Rev. B* **1976**, *13*, 5188-5192.

(10) Xia, J.; Chen, F.; Li, J.; Tao, N. *Nat. Nanotechnol.* **2009**, *4*, 505-509.

(11) Zimmermann, E.; Ehrenreich, P.; Pfadler, T.; Dorman, J. A.; Weickert, J.; Schmidt-Mende, L. *Nat. Photon*. **2014**, *8*, 669-672.

(12) Yoo, K., Kim, I.-Y., Lee, J. A., Kim, J. S., Lee, D. –K., Kim, K., Kim, J. Y., Kim, B., Kim, H., Kim, W. M., Kim, J. H., Ko, M. J. *ACS Nano*, **2015**, *9*, 3760-3771.

(13) Reynal, A.; Forneli, A.; Martinez-Ferrero, E.; Sa´nchez-Dı´az, A.; Vidal-Ferran, A.; O'Regan, B. C.; Palomares, E. *J. Am. Chem. Soc.* **2008**, *130*, 13558-13567.